Beyond Zeeman spectroscopy: Magnetic-field diagnostics with Stark-dominated line shapes

S. Tessarin,[1] D. Mikitchuk,[1] R. Doron,[1,a)] E. Stambulchik,[1] E. Kroupp,[1] Y. Maron,[1] D. A. Hammer,[2] V. L. Jacobs,[3] J. F. Seely,[3] B. V. Oliver,[4] and A. Fisher[5]

[1]*Faculty of Physics, Weizmann Institute of Science, Rehovot 76100, Israel*
[2]*Laboratory of Plasma Studies, Cornell University, Ithaca, New York 14853, USA*
[3]*Naval Research Laboratory, Washington DC 20375, USA*
[4]*Sandia National Laboratories, Albuquerque, New Mexico 87185, USA*
[5]*Faculty of Physics, Technion-Israel Institute of Technology, Haifa, Israel*

(Received 15 May 2011; accepted 27 July 2011; published online 6 September 2011)

A recently suggested spectroscopic approach for magnetic-field determination in plasma is employed to measure magnetic fields in an expanding laser-produced plasma plume in an externally applied magnetic field. The approach enables the field determination in a diagnostically difficult regime for which the Zeeman-split patterns are not resolvable, as is often encountered under the conditions characteristic of high-energy-density plasmas. Here, such conditions occur in the high-density plasma near the laser target, due to the dominance of Stark broadening. A pulsed-power system is used to generate magnetic fields with a peak magnitude of 25 T at the inner-electrode surface in a coaxial configuration. An aluminum target attached to the inner electrode surface is then irradiated by a laser beam to produce the expanding plasma that interacts with the applied azimuthal magnetic field. A line-shape analysis of the Al III 4s–4p doublet (5696 and 5722 Å) enables the simultaneous determination of the magnetic field and the electron density. The measured magnetic fields are generally found to agree with those expected in a vacuum based on the pulsed-power system current. Examples of other transitions that can be used to diagnose a wide range of plasma and magnetic field parameters are presented. © *2011 American Institute of Physics*. [doi:10.1063/1.3625555]

I. INTRODUCTION

Measurements of magnetic fields (B-fields) are of fundamental importance for studying laboratory and space plasmas. Common spectroscopic techniques for B-field measurements are based on Faraday rotation and the Zeeman effect. The Faraday-rotation technique, based on a B-field-induced anisotropy in the dispersion of the plasma, requires an external source of polarized light and gives information on the integral of the product of the electron density (n_e) and the B-field projection along the optical path of the external light beam. The Zeeman effect, which causes the splitting of spectral lines, gives the average B-field in the observed plasma volume and does not require a probe beam. In practice, particularly in high-energy-density plasmas, the Zeeman patterns are often completely smeared out due to the dominance of the Stark and Doppler broadenings. In such cases, when a preferred direction of the B-field exists, polarization spectroscopy can be applied to determine the B-field using a technique in which one detects the differences in the profile of a spectral line measured in orthogonal polarizations.[1] However, this technique involves the use of two identical spectrometers to measure the emitted spectrum from the same volume simultaneously. Since such an arrangement requires dividing the collected light into two spectrometers, it also results in the loss of at least half the photons in each of the recorded line profiles to be compared. However, a high signal to noise ratio is crucial due to the dominance of the other broadening mechanisms. A necessary condition for these measurements, and for those that are based on the Faraday effect, is a preferred direction of the B-field in the observation volume and during the time interval selected by the diagnostic system. However, when the B-field lacks a preferred direction, utilizing Faraday rotation or Zeeman splitting is either inapplicable or provides ambiguous results.

In a recent letter,[1] a new spectroscopic approach is described that enables the determination of B-fields when the Zeeman pattern is unresolved and which is not based on polarization spectroscopy. Furthermore, this method is applicable in cases of quasi-isotropic field distributions. While the principle underlying the new method is rather simple (see Sec. II), detailed line-shape calculations can give information on the plasma density and temperature in addition to the B-field.

The goal of the present work is to test and implement the new approach for rather high values of plasma densities (up to $\sim 10^{18}$ cm^{-3}) and B-fields (up to $\sim$20 T). In addition, we provide essential details on the new diagnostic method, as well as its applicability limits in terms of the field magnitude and plasma densities, explanation of the advantage of utilizing specific transitions for different plasma and field parameters, and a discussion on the error analysis in the field determination. As in the previous study,[1] we utilize the Al

a)Author to whom correspondence should be addressed. Electronic mail: ramy.doron@weizmann.ac.il.

III 4s–4p doublet transition (at 5696 and 5722 Å). The aluminum (Al) plasma is produced using a 7-ns laser that delivers a power density of 7×10^9 W/cm^2 to an Al target. When no external B-field is applied, the ablated plasma has an electron temperature (T_e) of a few electronvolts and an electron density $n_e \sim 10^{17}$ cm^{-3} at a distance of about 1 mm from the target. Under these conditions, Al atoms are ionized up to Al IV and their emission lines are predominantly in the visible-UV region. While the external B-field is produced by a microsecond pulsed-power system, the plasma expansion occurs over a time scale of tens of nanoseconds. Therefore, the plasma is effectively expanding in a quasi-static B-field. The presence of the applied B-field has major effects on the plasma-plume structure and dynamics, as can be inferred from the time-dependent line intensities and time-of-flight (TOF) measurements. In particular, we find that the B-field presence increases the plasma density significantly, enabling the extension of the plasma density measurements to $n_e > 10^{18}$ cm^{-3}. In this density range and for the B-fields generated in the present investigation, the line shapes of the Al III 4s–4p doublet are dominated by Stark broadening and the Zeeman pattern is not resolved, providing the conditions to test the new method.

In Sec. II, we provide a brief description of the diagnostic approach (further details of which are given in Ref. 1), and we expand on some relevant aspects of the line-shape modeling and the specific atomic system studied here. Sec. III describes the experimental setup and the spectroscopic system. The observations are described in Sec. IV, followed by a discussion of the results and sources of uncertainties in the measurements (Sec. V). Section VI presents examples of atomic systems suitable for the B-field measurement approach described here over a wide range of B-fields and plasma parameters. Conclusions are given in Sec. VII.

II. THEORETICAL METHOD

A. The principle of the B-field determination

The approach used for the B-field determination[1] employs two different fine-structure components of the same atomic multiplet. Each such component undergoes a different Zeeman splitting in the B-field, while the instrumental and the two other major line-broadening mechanisms, namely, the Stark and the Doppler effects, are practically identical for the two components. Therefore, if the multiplet components can be recorded simultaneously, the difference between their line shapes can be used for the determination of the B-field. Since the relative line intensities of the multiplet components are insensitive to the plasma parameters, their simultaneous recording ensures they are emitted from the same plasma regions (if opacity effects are negligible). Thus, variations of the plasma parameters along the line of sight do not affect the determination of the B-field.

Since the sign of the difference between the multiplet component widths is independent of the direction of the B-field, this method is also applicable to measurements when the direction of the B-field is either unknown or is known to have no preferred direction (e.g., when the field direction changes significantly in the region viewed or during the time of observation). An uncertainty in the direction of the B-field results in an associated uncertainty in the inferred field magnitude (see Discussion in Sec. V). However, if the field direction is known (as is the case in the present study), the accuracy of the inferred B-field is limited only by the error bars of the data points. The elimination of the direction uncertainty allows detailed line-shape modeling to yield information also on the spatial profile of the plasma electron density.

B. Utilizing the Al III 4s–4p doublet transition

Generally, the $^2S - {}^2P$ system is a favorable candidate for the proposed diagnostics since the relative line-width *difference* between the doublet components $^2S_{1/2} - {}^2P_{1/2}$ and $^2S_{1/2} - {}^2P_{3/2}$ is the most sensitive (relative to other types of transitions) to B-fields. Specifically, for the present study we utilize the Al III $2p^6 4s - 2p^6 4p$ doublet, with its two components 4s $^2S_{1/2}$ – 4p $^2P_{3/2}$ at 5696.6 Å and 4s $^2S_{1/2}$ – 4p $^2P_{1/2}$ at 5722.7 Å. As explained next, the energy difference between the two fine-structure components is suitable for performing the B-field and electron density measurements in the experiment.

The usefulness of the $^2S_{1/2} - {}^2P_{1/2,\,3/2}$ doublet for performing the line-width comparison requires that its components are spectrally resolved. In the present experiment, the Stark broadening is expected to be the dominant broadening mechanism. Calculations of the Stark broadening show that the two Al III 4s – 4p components are clearly separated (without the B-field) up to $n_e \approx 3 \times 10^{18}$ cm^{-3}. For any density below 3×10^{18} cm^{-3}, there is a range of B-fields for which the diagnostic is applicable. The upper bound of this range is determined by the condition that the two components remain separated in the presence of a B-field. For example, for $n_e = 10^{18}$ cm^{-3}, in the presence of B-fields larger than about 40 T the two components are difficult to separate. The lower bound is determined by the condition that the width difference between the two components can still be clearly detected; namely, the width-difference relative to the average line width should be sufficiently large. For example, at $n_e = 10^{18}$ cm^{-3}, a B-field of ~7 T induces a width difference of about 0.3 Å, which is less than 5% of the average line-width (7 Å), making an accurate B-field measurement effectively impossible below this limit.

Selecting the Al III 4s–4p transitions has two additional important advantages. The Al III charge state and upper levels of the transition are expected to be appreciably populated in the plasma produced here, and opacity effects that may complicate the analysis are expected to be small, since the Al III ground state is not involved in the transitions. Furthermore, in the presence of the B-field, opacity becomes negligible due to the additional Zeeman broadening.

C. Line-shape modeling

For the line-shape calculations, we employ the computational method[2] that takes into account, in an *ab initio* manner, both the B-field effect and the Stark broadening and shift. The Doppler and the instrumental broadenings are accounted for by performing convolutions with the respective profiles, although for the present plasma conditions, these two sources of line broadening provide negligible contributions.

In a general case, the modeling can be applied to describe a distribution of plasma parameters. A simple case of multicomponent-plasma parameters corresponds to light emitted from two regions with different electron densities $n_e^{(1)}$ and $n_e^{(2)}$ (since the dependence on the temperature is rather weak, we further assume $T_{e.i}^{(1)} = T_{e.i}^{(2)} = T$) but with the same B-field,

$$I(\omega) = I_0 + c^{(1)} I(B, T, n_e^{(1)}; \omega) + c^{(2)} I(B, T, n_e^{(2)}; \omega), \quad (1)$$

where I_0 is the background signal and $c^{(1)}$ and $c^{(2)}$ are weight coefficients to be determined, together with the values of B, T, $n_e^{(1)}$, and $n_e^{(2)}$, by varying their values until a best fit of $I(\omega)$ to the measured spectrum $I_m(\omega)$ is achieved.

Obtaining a good fit requires many runs of the line-shape calculation code for different combinations of the fitting parameters (B, T, $n_e^{(1)}$, $n_e^{(2)}$, $c^{(1)}$, $c^{(2)}$, I_0). Using resource-demanding computations[1] directly in this context is not practical. Instead, if the Stark and Zeeman effects can be assumed to be independent, the total line profile can be expressed as a convolution of the two profiles,

$$I(B, T, n_e; \omega) = \int d\omega' I_Z(B, \omega') I_S(T, n_e, \omega - \omega'), \quad (2)$$

where the (static) Zeeman pattern $mI_Z(B;\omega')$ is calculated using a fast code[3] and the Stark profile $I_S(T, n_e; \omega)$ is assumed to be a shifted Lorentzian (i.e., an isolated line shape in the impact approximation[4]),

$$I_S(T, n_e; \omega) = \frac{1}{\pi} \frac{w(T, n_e)}{[\omega - \omega_0 - d(T, n_e)]^2 + w^2(T, n_e)}. \quad (3)$$

Here, $w(T,n_e)$ and $d(T,n_e)$ are, respectively, the Stark half-width at half-maximum (HWHM) and the shift parameters, and ω_0 is the unperturbed line position. Both $w(T, n_e)$ and $d(T,n_e)$ depend linearly on n_e, allowing for simple factorizations to be used: $w(T,n_e) = n_e w'(T)$, $d(T,n_e) = n_e d'(T)$. We note that the isolated-line approximation is valid for the case of the Al III 4s – 4p line discussed here, since the Stark broadening under the plasma conditions considered ($\sim$20 cm^{-1}) is about three orders of magnitude smaller than the distance to the closest levels responsible for the Stark broadening. Therefore, the isolated-line approximation, namely, the approximation in which the Stark contribution to the shape is a shifted Lorentzian with width and shift that depend linearly on n_e, should work very well. This indeed was proved by *ab initio* calculations[3] (with $B = 0$) that also provided the $w'(T)$ and $d'(T)$ dependence on T (found to be rather weak); the actual values are calculated in advance on a grid of T values and used in a fast lookup/interpolation scheme during the fitting procedure.

The validity of the approximation in Eq. (2) was checked by comparing the line shape obtained using this expression with the result of a detailed calculation for a few sets of B, n_e, and T. A typical result is given in Fig. 1. The differences between the two sets of line-shapes are barely detectable. We note that for the rather high magnetic fields

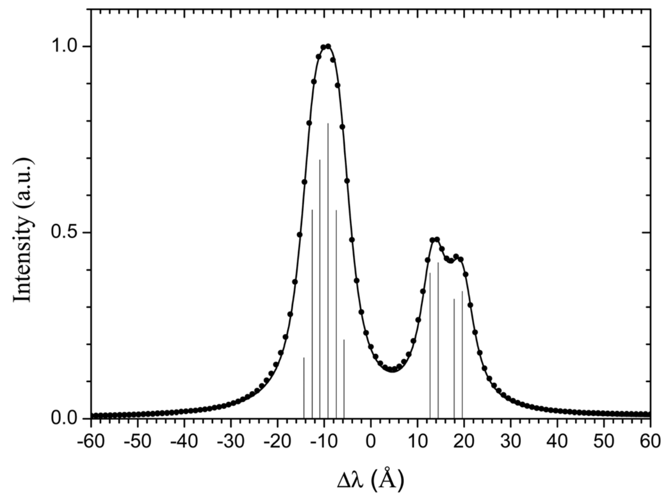

FIG. 1. Comparison of the line-shapes of the Al III 4s–4p doublet calculated including the effect of a static magnetic field of 17 T, Stark broadening due to an electron density of $n_e = 10^{18}$ cm^{-3}, and an electron temperature of $T_e = 4$ eV. Circles: *ab initio* calculations using the method in Ref. 1; solid line: with the effect of the magnetic field factorized according to Eqs. (2) and (3). Also shown is the theoretical Zeeman pattern with no line broadening. The term $\Delta\lambda = 0$ corresponds to the weighted-average wavelength of the doublet (5707 Å).

investigated in the present study, the magnetic-field-induced perturbation of the energy levels is not small compared to the fine structure energy splitting of the Al III 4p level. Therefore, the deviations from the linear Zeeman effect become noticeable, resulting in an asymmetry of the Zeeman pattern of the 4s–4p doublet components.

III. EXPERIMENTAL SETUP

The experimental setup is designed to enable systematic measurements for plasmas with electron densities and external B-fields, respectively, in the ranges of 10^{16}–10^{18} cm^{-3} and up to 25 T. A current-pulse (rise-time of 1.7 μs) with a peak value of 270 kA, measured with absolutely calibrated B-dot probes with an accuracy better than 10%, was driven axially through a coaxial low-inductance transmission line in vacuum (10^{-5} Torr), generating an azimuthal B-field, as shown in Fig. 2. The transmission line consists of a cylindrical inner electrode and four return current posts at a radius of 3.5 cm. The inner electrode, terminated with a cut-off cone, is connected to a 2-cm long, 4-mm diameter rod, and four radial bars that connect to the return current posts (see enlarged portion of Fig. 2). An Al target, attached to the middle of the 2-cm rod, is irradiated by a Nd-YAG laser beam (7 ns, 100 mJ, 7×10^9 W/cm^2), producing the plasma plume that interacts with the B-field. At the time of the peak current, a B-field of 25 T is produced at the surface of the rod. The currents flowing through the return-current bars provide only a very small ($\sim$1% or less) contribution to the B-field at the relevant distances of several mm from the target.

The diagnostic system consists of a 1-m, visible-UV spectrometer coupled either to a gated intensified charge-coupled device (ICCD) camera or to a fast photomultiplier (PMT). The spectra recorded by the ICCD camera give simultaneous coverage of a 30-Å spectral window with 0.4-Å resolution for

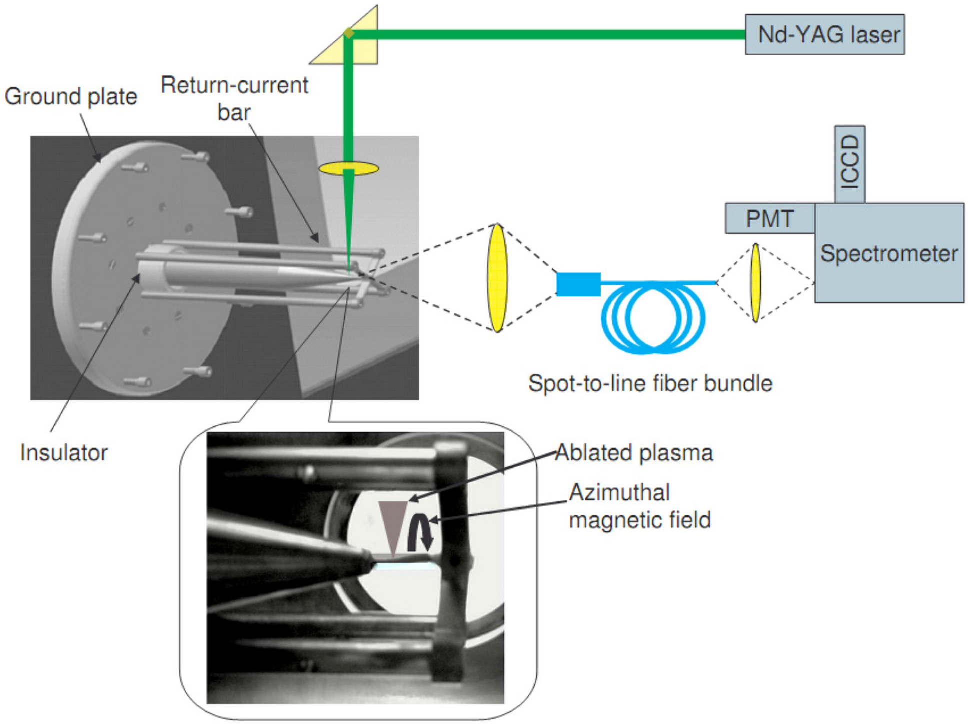

FIG. 2. (Color online) Schematic diagram of the experimental set-up inside the vacuum chamber. The inset shows a zoom of the conical inner electrode and its connection to the return current bars by a 4 mm diameter rod. The laser ablation occurs on an Al target in the middle of the connecting rod in the presence of the azimuthal B-field.

the wavelength range of interest, and are used for the line-shape analysis. The PMT gives the time-dependent (5-ns resolution) intensities of selected spectral lines that are used mainly for time-of-flight measurements that are needed to optimize the line intensities for the high-spectral-resolution measurements. The plasma is viewed along the axial direction of the transmission line and perpendicular to the azimuthal B-field. The light is collected by a lens coupled to a 380-μm diameter fiber-optic bundle. The optical arrangement with a magnification of 1 and f-number of 10, collecting the light from a plasma column ~1.5-mm wide (determined from white light images), provides a spatial resolution of 0.5 mm along the radial direction (including an uncertainty of 0.5 mm in the position of the focus). We note that in the field-free expansion the plasma width along the line-of-sight is much larger (~5 mm in the relevant times) since its motion is not limited in the axial direction by the B-field (see also Ref. 2), yielding a total resolution of ~0.65 mm.

The experimental setup provides considerable flexibility in the B-field measurements. Since the rise-time of the current is an order of magnitude longer than the expansion time of the laser-ablated plume (about 150 ns for the relevant distances), the plume is effectively expanding in the presence of a quasi-static B-field distribution. Therefore, the selection of the B-field magnitude that interacts with the plasma at each radial distance is controlled by selecting the appropriate time delay between the application of the current and the triggering of the laser.

IV. MEASUREMENTS

A. Time-of-flight measurements

Time-of-flight measurements are used here to determine the times at which the Al III 4s–4p peak-intensity emission is obtained at different distances from the target surface in order to maximize the signal-to-noise ratio in the B-field measurements. TOF measurements were performed with and without the application of the external B-field. Figure 3(a) presents the time-evolution of the Al III 5696 Å peak-normalized intensity during the free expansion of the plume at various radial distances from the ablation surface. The plasma emitting the Al III peak intensity expands with a velocity of about 6×10^6 cm/s, in agreement with other studies under similar conditions.[6,7] Figure 3(b) shows similar data obtained for expansion in the presence of the external B-field. In this case, the plasma emitting the Al III peak intensity appears to have an expansion velocity that is lower, about 3×10^6 cm/s. The slower expansion rate suggests that the plasma density might be higher relative to the case of free expansion. Indeed, the line-shape analysis shows that for free expansion the n_e at peak intensity decreases from about 3×10^{17} cm^{-3} down to about 10^{16} cm^{-3} between 1 mm and 5 mm; by contrast, in the presence of the B-field, the densities at peak intensity at each distance are about a factor of 3 higher. In both cases, lower density plasmas can be achieved by reducing the laser power-density.

The TOF curves are also used for selecting the integration time (gating) applied to the ICCD camera. Obviously, long ICCD gating would improve the photon statistics of the recorded spectra. However, long gating necessarily results in an undesired integration over light emission from time-varying densities. In order to ensure that the spectra are recorded from a limited density distribution, we set the gating in each measurement to be equal to the time duration in which the TOF signal is $\geq 90\%$ of its peak (assuming the light intensity is correlated mainly with n_e). For example, in Fig. 3(b) we show the interval of 25 ns corresponding to the gating applied in the measurement made 1 mm from the target.

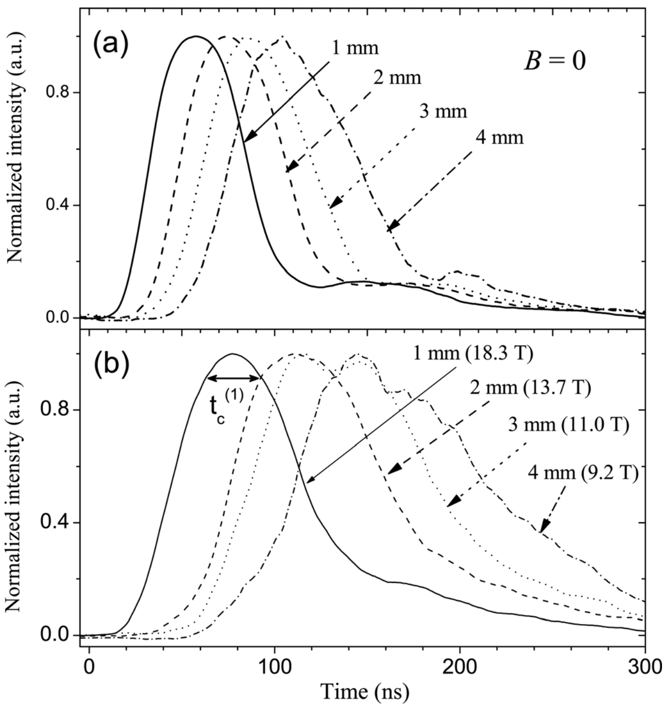

FIG. 3. Temporal evolution of the Al III 5696-Å line intensity recorded from various distances from the target for the free-field case (a) and in the presence of the external B-field (b). Time 0 corresponds to the time the laser beam first hits the Al target. In (b), the numbers in parentheses indicate the expected B-field at each distance, based on the current measurement. The interval $t_c^{(1)}$ represents the gating of the ICCD camera used in the measurement for a distance of 1 mm from the target.

B. Magnetic-field measurements

The measured line-shapes of the Al III 4s–4p doublet (5696 and 5722 Å) at different distances from the target (with the center of the coaxial line defined as $r = 0$) in the presence of the B-field, together with their simulations, are presented in Figs. 4–6. These figures demonstrate the transition from a Zeeman-splitting-based diagnostic to the multiplet-comparison diagnostic, as discussed in Sec. II. At relatively large distances from the target (see Fig. 4), where the emission is produced from a relatively low-density plasma (leading to a relatively small Stark broadening), both components of the doublet reveal spectral profiles that exhibit Zeeman splitting. Closer to the target, the higher densities cause the line shapes to be Stark-dominated, and the Zeeman pattern is smeared out. In the spectrum emitted 2 mm from the target ($r = 4$ mm, see Fig. 5), the Zeeman pattern of the stronger $^2S_{1/2} - {}^2P_{3/2}$ component is completely smeared out, although it is still noticeable in the shape of the weaker $^2S_{1/2} - {}^2P_{1/2}$ component. For $r = 3$ mm (see Fig. 6), the Zeeman patterns of both spectral components are completely smeared out. In this case, only the use of the present method reveals the presence of the B-field. To clearly demonstrate the effect of Stark broadening, Figs. 4–6 also show the calculated Zeeman patterns at each distance assuming zero electron density but broadened by a Gaussian to account for the expected Doppler and instrumental broadenings.

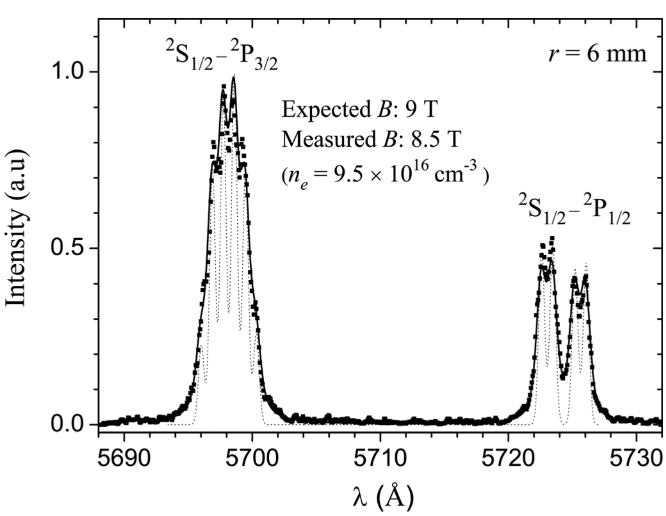

FIG. 4. The Al III 4s–4p doublet (5696 and 5722 Å) recorded at $r = 6$ mm (squares). The calculated broadened spectrum (solid curve) that best matches the experimental data yields an electron density of 9.5×10^{16} cm^{-3} and a field of 8.5 T compared to an expected field of 9 T. The dotted line represents the corresponding zero-density Zeeman pattern.

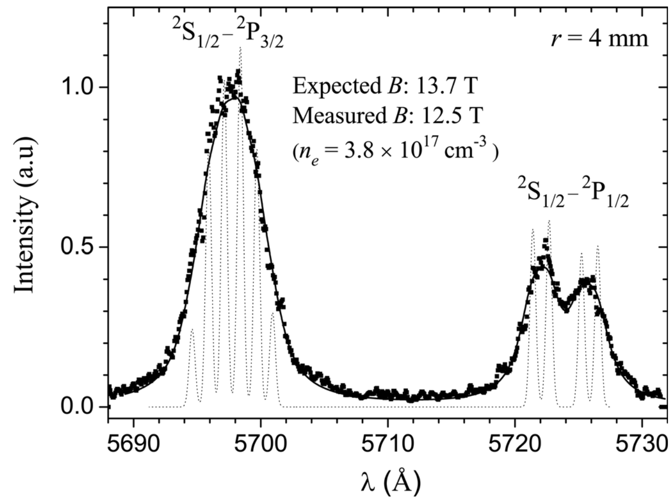

FIG. 5. Same as in Fig. 4, for $r = 4$ mm results.

The B-fields and the electron densities are obtained using modeling of the measured line-shapes. The multiplet line-shapes are dominated by Stark broadening and the line-

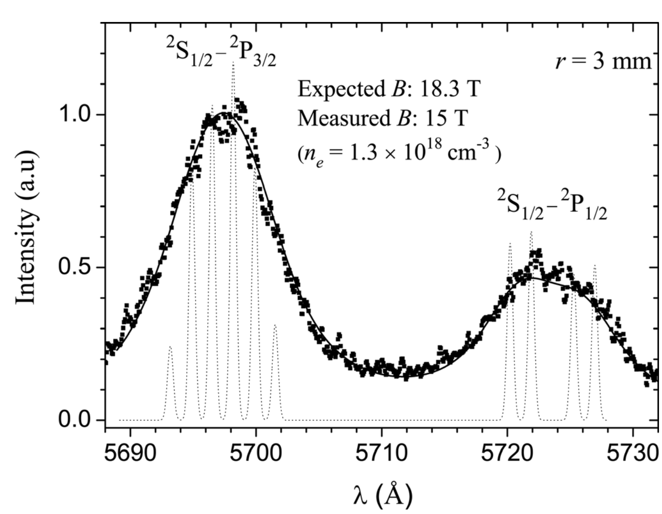

FIG. 6. Same as in Fig. 4, for $r = 3$ mm.

widths difference depends upon the B-field. The calculated spectral profiles shown in Figs. 4–6 include the contributions of the Zeeman, Stark, and Doppler effects, as well as instrumental broadenings to the line-shapes. The modeling process consists of two steps. The calculated Zeeman pattern[1] is convolved with a Voigt profile, where the Lorentzian part corresponds to the Stark broadening, and the Gaussian part corresponds to the sum of the Doppler (see next paragraph) and instrumental broadenings. The input values of B, n_e, and T are then varied until the least-squares best fit to the experimental curve is obtained, allowing for their simultaneous determination.

Assuming $T_i \approx T_e$ (where T_e is several eV, obtained from collisional-radiative calculations and in agreement with other experiments[6]), the thermal Doppler broadening is negligible compared to the measured instrumental broadening of 0.4 Å. The Doppler broadening that arises from the non-thermal ion-kinetic spread is $\sim$1 Å, inferred from the B-free line-shape measurements at large distances from the target (>4 mm) where the Stark broadening is small. This broadening is consistent with the typical ion velocities as determined from the TOF measurements. However, under the influence of the B-field, line-shape calculations that agree best with observations are obtained with a Gaussian component that is close to the instrumental broadening, i.e., in the B-field, the ion-kinetic broadening due to the motion in the observation direction is small compared to the instrumental broadening (apparently due to a limitation of the plasma motion along the cylindrical axis induced by the B-fields[2]). In particular, we find that for the line-shapes recorded from the dense plasma, at distances up to about 2 mm from the target, even the field-free Doppler broadening that is considered as an upper bound of the Doppler contribution, is very small compared to the Lorentzian part. Therefore, accurate knowledge of the Doppler broadening (assumed to be a Gaussian also in the B-field) is unimportant for the modeling of the present results.

The uncertainties of the measured B-fields in the low-density region are determined from the uncertainties in the positions of the Zeeman-split peaks and are estimated to be $\pm$ 6%. In the high-density region, where the determination of B is based on fitting the doublet line-shape, the uncertainty depends on the sensitivity of the modeling to variations in B and n_e. Since the Stark broadening is the dominant broadening mechanism, the uncertainty of the measured B is larger in the high-density region. For the spectrum recorded from $r = 3$ mm, the best fit is obtained for $B = 15$ T and $n_e = 1.3 \times 10^{18}$ cm^{-3}. To examine the uncertainties, comparisons are made of the experimental spectrum to synthetic line-shapes, obtained by varying B and finding n_e that gives the best fit for each B. An example of such a comparison is given in Fig. 7, where the experimental spectrum is shown with three modeling results for $B = 9$, 15, and 20 T. By closely examining the differences between the theoretical and the experimental line-shapes, particularly in the spectral ranges marked by the rectangular frames, it can be seen that the line-width obtained with 20 T is too wide to explain the experimental data, whereas that obtained with 9 T is too narrow.

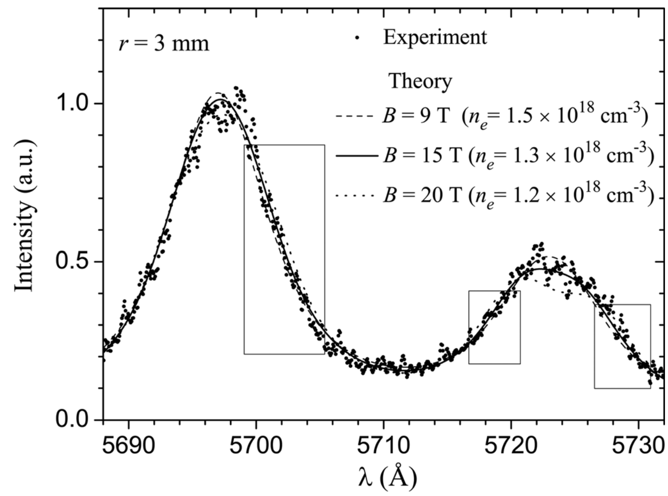

FIG. 7. Calculated line shapes of the Al III 4s–4p doublet (5696 and 5722 Å) calculated for three different B-fields (9, 15, and 20 T) and electron densities that give the best fits for each B-field value, compared to the experimental spectrum obtained for $r = 3$ mm.

As can be seen from Figs. 4–6, the measured B-fields are rather close to those expected from the measured current, although they are persistently smaller. Figure 8 presents the $1/r$ dependence of the measured B-field compared to the expected value in vacuum. While we cannot rule out a diamagnetic effect in which the B-field is partially excluded from the plasma, the nearly $1/r$ linear dependence of the measured B-field suggests a systematic error. Plausible sources of such systematic errors are the determination of the absolute distance from the target and the absolute calibration of the B-dot probes used for the current measurements.

C. Low-spatial resolution spectra

Since one of the purposes of the present work is testing the diagnostics under various scenarios, we performed measurements that simulate common situations in which the diagnostic system records emission from a plasma with a wide range of densities and B-fields. In these measurements, spectra were recorded with a lower spatial resolution of 1.5 mm

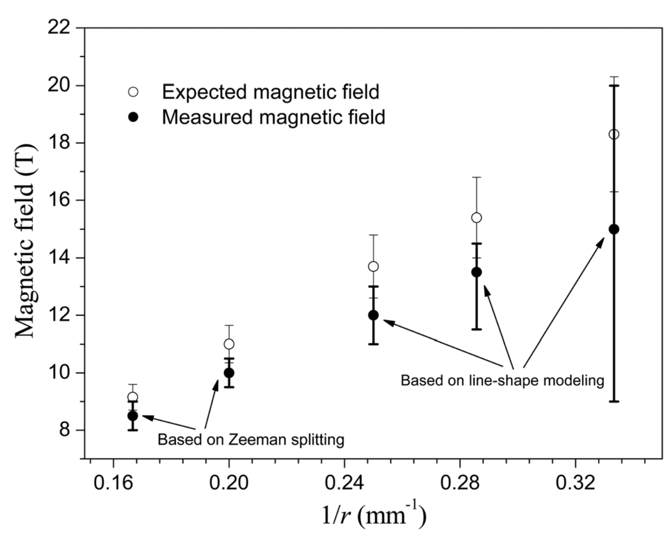

FIG. 8. Expected and measured B-field as a function of $1/r$.

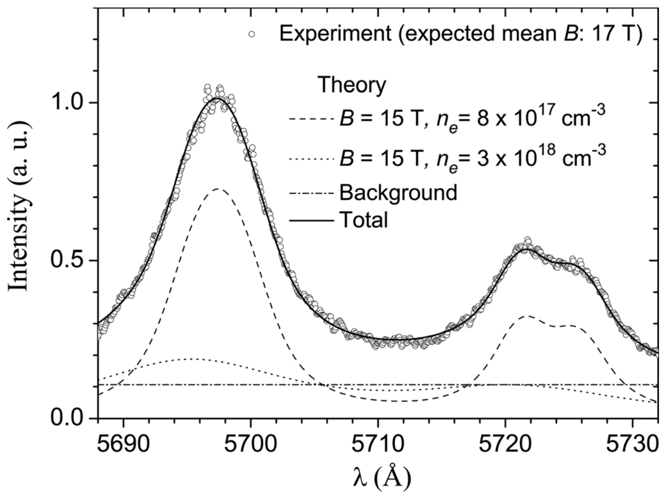

FIG. 9. The Al III 4s–4p doublet (5696 and 5722 Å) recorded at 1.5 mm from the target surface ($r = 3.5$ mm) with a spatial resolution of 1.5 mm, and the calculated result based upon an assumption of a combination of two different density regions that best reproduces the data, together with the specific result from each of those regions.

(compared to 0.5-mm resolution presented in the above results). Figure 9 presents such an Al III 4s–4p spectrum from a region centered at $r = 3.5$ mm, where the predicted B-field varies between 12.7 and 19.6 T. A line-shape analysis shows that *no* reasonable combination of a single B-field and a single n_e can satisfactorily fit the experimental curve. In particular, the wings of the spectral lines are not well reproduced. Instead, considering multiple density values leads to good agreement with the experimental results. The theoretical curves in Fig. 9 show the full calculation (labeled "total") and its components. It is obtained using $B = 15$ T and emission from two plasma components, $n_e = 8 \times 10^{17}$ cm^{-3} and 3×10^{18} cm^{-3}, with respective fractions of $c^{(1)}$:$c^{(2)} = 1.8$: 1 [see Eq. (1)] superimposed on a constant background. The latter is likely due to continuum emission originating from the target surface.

This finding is plausibly due to the fact that the measurement integrates over a region with a large density gradient, each part of which gives rise to a different Stark broadening, which cannot be reproduced by a line-shape that corresponds to a single mean density. The fact that a single mean B-field can be used to produce a good fit to the experimental result is a consequence of the dominance of the Stark broadening. Indeed, the simulation results are not sensitive to the B-field assumed for the *high-density* component, and it is only the B-field assigned to the *low-density* component that can be determined. The inferred B-field of 15 T is in agreement with the range of fields in the region viewed. Weighing the calculated field distribution by the spatial distribution of the Al III intensity (obtained from the high spatial-resolution measurements), and assuming a spatial resolution of 1.5 mm (FWHM) centered at $r = 3.5$ mm, yields a mean predicted B-field of 17 T.

V. ERROR ANALYSIS FOR UNKNOWN B-FIELD CONFIGURATION

In the analysis presented above, we have assumed that the B-field maintains its vacuum azimuthal symmetry inside

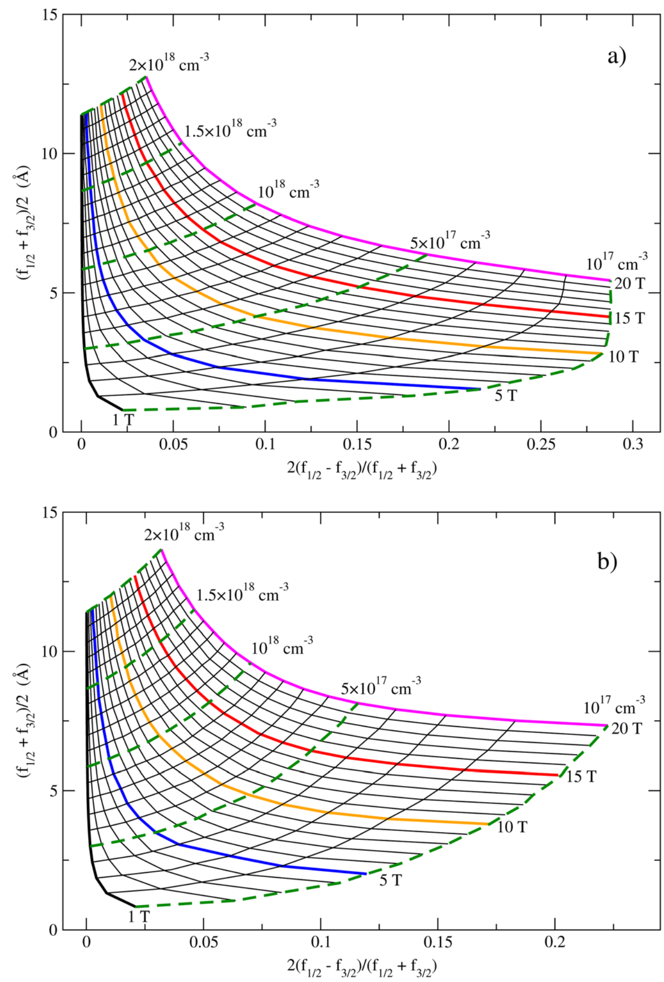

FIG. 10. (Color online) The Al III 4s–4p doublet average line-width, $(f_{1/2}+f_{3/2})/2$, as a function of the relative line-width difference, $2(f_{1/2}-f_{3/2})/(f_{1/2}+f_{3/2})$, calculated for various electron densities and B-fields for the case of perpendicular field (a) and parallel field (b) relative to direction of observation. The line-width, f, refers to full-width-half-area.

the plasma. The fact that the measured B-fields are found to be close to those expected in vacuum, indeed shows that an azimuthal field provides an adequate representation of the field inside the plasma. However, a predominant field direction does not always exist, or it could be unknown. Here we consider the effect of such cases on the analysis and the field determination.

The additional uncertainty in the field determination, which is due to non-uniformity in the field direction or to lack of information on the field direction, can be estimated by considering the two extreme cases: (i) a field directed perpendicular to the line of sight ($B_\perp$) and (ii) a field aligned along the line of sight ($B_\parallel$). For each of these cases, Fig. 10 shows the average line-width of the Al III 4s–4p doublet as a function of the relative width-difference, calculated for various electron densities and B-fields. The line-widths in Fig. 10 refer to the *full-width-half-area* (FWHA)[8] and not to the more common definition of full-width-half-maximum (FWHM). We choose this presentation to avoid the ambiguities that may arise in determining the FWHM when the Zeeman-splitting is partially resolved or in the cases of high B-field, where the B-field effect on the spectral lines is not small compared to the fine structure splitting, resulting in noticeable asymmetric line-shapes.

As an illustration of the effect of an unknown B-field direction on the measured B-field, let us consider the spectrum obtained from $r = 3$ mm (see Fig. 6). The average FWHA is 8.6 Å and the relative width difference is 4.1%. For the case of $B_\perp$ (Fig. 10(a)), these values reproduce the results found in Sec. IV B, $B = 15$ T and $n_e = 1.3 \times 10^{18}$ cm^{-3}. However, assuming that the field is aligned along the line of sight (Fig. 10(b)), one obtains $B = 14$ T and $n_e = 1.1 \times 10^{18}$ cm^{-3}. Thus, the uncertainty associated with the lack of information on the field direction in this case is only a few percent, which is much less than that due to the uncertainty in the experimental points, as estimated in Sec. IV B.

It is important to emphasize that the B-field diagnostic does not require independent knowledge of n_e. The lower n_e obtained when assuming $B_\parallel$ only reflects the wider Zeeman pattern that is induced when the B-field is aligned along the line of sight, compared to that when a B-field of the same magnitude is directed perpendicular to the line of sight. A wider Zeeman pattern requires a convolution with a narrower Lorentzian to satisfy the best fit criterion, which implies a lower value of n_e.

VI. TRANSITIONS FOR DIAGNOSING VARIOUS PLASMA AND B-FIELD PARAMETERS

A prerequisite for employing the new B-field diagnostic method is a resolved fine-structure splitting structure. A partial overlapping between the doublet components, here seen in the spectrum recorded at 1 mm away from the laser target ($r = 3$ mm, see Fig. 6), demonstrates that in this experiment the Al III 4s–4p transition is not adequate for probing regions closer than 1 mm to the target. For various experiments, other atomic systems can be suggested to cover different ranges of plasma and B-fields parameters. Examples of such systems are given in Table I. This table presents a list of 3s–3p doublet transitions in selected ions pertaining to the Li-like isoelectronic sequence, together with the maximum B-field and n_e values for which the diagnostic is applicable using that specific ion species. The criterion here used for the maximum B-field is that the average Zeeman width of the two doublet components should be equal to 70% of the fine-structure splitting, ensuring a resolved fine structure for densities that induce Stark profiles of similar widths. The limitation on n_e may arise either from the Stark width that may smear out the fine structure, or from the continuum level that may be comparable to the transition intensities. In the first case, the criterion for the maximum n_e here adopted is that the Stark width should be equal to 70% of the fine-structure splitting, and in the second case it is that the continuum level should be 20% of the peak spectral density of the weaker doublet component. For evaluating the n_e-restriction due to the continuum level, steady-state calculations of the intensities of the transitions given in Table I and the continuum at the relevant wavelength in each ion are performed. For C IV, O VI, and Ne VIII, the continuum and line intensities are calculated for electron temperatures corresponding to 10% of the ionization potentials, and for Mg X, Si XII, and Ar XVI, the calculations are performed for temperatures corresponding to 20% of the ionization potentials. At these electron temperatures, the respective ions are expected to be significantly abundant. Under these assumptions, we find that for all the transitions in Table I, the maximum n_e that limits the diagnostics due to the continuum level is about 10^{19} cm^{-3}. It should be noted that if the conservative criterion of a continuum level that is 20% of the peak line intensity is relaxed and it is allowed to be equal to the peak line intensity, then the maximum n_e rises to $\sim 3 \times 10^{19}$ cm^{-3}. It can be seen from the Table that for the relatively low charge-state ions the Stark width imposes a more severe limitation on n_e, whereas for the higher charge states n_e is restricted by the continuum level. Similarly to the Al III 4s–4p transition used here, the ground state is not involved in the Li-like 3s–3p transition, thus opacity effects are not expected to hamper the diagnostic method.

As is evident from Table I, the 3s–3p doublets offer B-field diagnostics for a variety of applications. An example is utilizing Ne VIII transitions for diagnosing the tens-Tesla field of MA z-pinches during the implosion. Another example is the use of the 3s–3p doublets in C IV, N V, and O VI for diagnosing the B-fields in particle-beam diodes with typical parameters of $B \sim 10$ T, $T_e \sim 10$ eV, and $n_e \sim 10^{18}$ cm^{-3}.

TABLE I. Selected 3s – 3p doublet transitions of Li-like ions potentially useful for B-field measurements. E_I is the ionization potential. Max. B and Max. n_e are the calculated upper limits for which the new diagnostic method is applicable for each transition. The maximum n_e given in the table is calculated considering the restriction due the Stark broadening being comparable to the fine-structure splitting. The maximum n_e due to the continuum level is calculated to be $\sim 10^{19}$ cm^{-3} for all the transitions in the table, imposing a more severe restriction on n_e than that due to Stark except for C IV (underlined).

Ion	E_I (eV)	λ (Å)		Max. B (T)	Max. n_e (cm^{-3}) due to Stark
C IV	65	5801	5811	14	$\underline{2 \times 10^{18}}$
O VI	138	3811	3834	50	3×10^{19}
Ne VIII	239	2820	2860	200	1.5×10^{20}
Mg X	368	2215	2281	500	7.5×10^{20}
Si XII	523	1803	1884	1000	2.4×10^{21}
Ar XVI	918	1282	1421	3500	2.2×10^{22}

VII. CONCLUSIONS

A spectroscopic method for the determination of magnetic fields,[2] applicable in situations where the Zeeman splitting patterns are not resolved (either due to the field variation in space and time, or due to the dominance of other line broadening mechanisms), is implemented in a study featuring an aluminum laser-produced plasma expanding in the presence of externally applied B-fields. The method is shown to be essential for B-field measurements in regions near the laser target, where the Stark-dominated line shapes prohibit the use of the traditional Zeeman spectroscopy. The line-shape analysis of the Al III 4s–4p doublet enables the simultaneous determination of the B-field and the electron density. In addition, the line-shape analysis is shown to be a powerful tool for obtaining information on the electron density distribution. This is demonstrated by the analysis of spectra obtained with relatively poor spatial resolution, exhibiting line shapes that can be only explained by the presence of a substantial plasma-density gradient. The measured B-fields in the plasma are found to be consistently smaller by about 10% than those expected in vacuum. The accuracy of the measurements is insufficient to determine whether these results arise from plasma diamagnetic effects.

ACKNOWLEDGMENTS

The authors are grateful to R. W. Lee and K. Tsigutkin for their valuable suggestions and to P. Meiri for his skilled technical assistance. This work was supported in part by the U.S.-Israel Bi-national Science Foundation (BSF) and by NRL (USA), Contract number N173-09-2-C010. D.A.H. was partially supported by the Stewardship Sciences Academic Alliances program of the National Nuclear Security Administration under DOE Cooperative Agreement No. DE-FC03-02NA00057. V.L.J. was partially supported by the U.S. Office of Naval Research.

[1]E. Stambulchik, K. Tsigutkin, and Y. Maron, Phys. Rev. Lett. **98**, 225001 (2007).
[2]E. Stambulchik and Y. Maron, J. Quant. Spectrosc. Radiat. Transf. **99**, 730 (2006).
[3]E. Stambulchik and Y. Maron. Phys. Rev. A **56**, 2713 (1997).
[4]H. R. Griem, *Spectral Line Broadening by Plasmas* (Academic, New York, 1974).
[5]C. Plechaty, R. Presura, S. Stein, D. Martinez, S. Neff, V. Ivanov, and Y. Stepanenko, High Energy Density Phys. **6**, 258 (2010).
[6]S. S. Harilal, M. S. Tillack, B. O'Shay, C. V. Bindhu, and F. Najmabadi, Phys. Rev. E **69**, 026413 (2004).
[7]S. Gurlui, M. Agop, P. Nica, M. Ziskind, and C. Focsa, Phys. Rev. E **78**, 026405 (2008).
[8]M. A. Gigosos, M. A. Gonzalez, and V. Cardenoso, Spectrochim. Acta, Part B, Surf. Sci. **58**, 1489 (2003).